Observer-Based Control of *LLC* DC/DC Resonant Converter Using Extended Describing Functions

Concettina Buccella, *Senior Member, IEEE*, Carlo Cecati, *Fellow, IEEE*, Hamed Latafat, *Student Member, IEEE*, Pierdomenico Pepe, *Senior Member, IEEE*, and Kaveh Razi, *Student Member, IEEE*

***Abstract*—This paper presents theoretical and practical results about dynamic analysis, frequency response, and control of a *LLC* resonant dc/dc converter operating under wide input voltage and load variations. A nonlinear model for the *LLC* resonant converter was developed using the extended describing function method; then, based on the derived model, a nonlinear observer-based controller was designed and implemented with a digital signal processor. Transient responses obtained under input voltage and output load variations show that the proposed controller is capable to stabilize the output effectively. Experimental results prove the superiority of the proposed observer-based controller over a conventional PID controller.**

***Index Terms*—DC/DC power conversion, digital control, extended describing functions (EDFs), nonlinear systems, observers, renewable energy systems, resonant power conversion, state feedback.**

NOMENCLATURE

A_s	Network analyzer source signal amplitude.
C_f	Output capacitor.
C_s	Series resonant capacitor.
$\triangle$	Sampling period.
f_r	Resonant frequence.
f_s	Network analyzer source signal frequency.
$f_{\rm VCO}$	Voltage-controlled oscillator frequency.
i_c	Cosine components of the transformer secondary current.
i_m	Magnetizing current.
i_{mc}	Cosine components of the magnetizing current.
i_{ms}	Sine components of the magnetizing current.
i_p	Transformer primary current.
i_r	Series resonant current.
i_{rc}	Cosine components of the series resonant current.
i_{rs}	Sine components of the series resonant current.
i_s	Sine components of the transformer secondary current.
k	Sampling number.
K_D	Derivative gain parameter of the PID controller.
K_I	Integral gain parameter of the PID controller.
K_P	Proportional gain parameter of the PID controller.
L_m	Magnetizing inductance.
L_s	Series resonant inductance.
n	Transformer ratio.
R	Output load.
r_s	Internal resistance of the series resonant inductance.
T_s	Sampling time.
V_c	Series capacitor voltage.
v_{cc}	Cosine components of the series capacitor voltage.
V_{cf}	Output voltage.
v_{cs}	Sine components of the series capacitor voltage.
$V_{\rm dc}$	Input dc voltage.
$V_{\rm in}$	Square wave voltage applied to the resonant tank.
ω_s	Switching frequency of the converter.

Manuscript received July 15, 2014; revised September 23, 2014; accepted October 27, 2014. Date of publication November 14, 2014; date of current version May 22, 2015. Recommended for publication by Associate Editor M. Ordonez.

C. Buccella and C. Cecati are with the Department of Information Engineering, Computer Science and Mathematics, DigiPower s.r.l, University of L'Aquila, 67100 L'Aquila, Italy (e-mail: concettina.buccella@univaq.it; carlo.cecati@univaq.it).

H. Latafat, P. Pepe, and K. Razi are with the Department of Information Engineering, Computer Science and Mathematics, University of L'Aquila, 67100 L'Aquila, Italy (e-mail: hamed.latafat@univaq.it; pierdomenico.pepe@univaq.it; kaveh.razi@univaq.it).

Color versions of one or more of the figures in this paper are available online at http://ieeexplore.ieee.org.

Digital Object Identifier 10.1109/TPEL.2014.2371137

I. INTRODUCTION

RESONANT dc/dc converters are gaining popularity and applications due to their capability to operate at zero-voltage switching (ZVS) condition [1]. This mode ideally eliminates switching losses, thus resulting increased efficiency in comparison with hard switching converters, in which power devices are commutated without taking into account instantaneous volt/ampere values, thus resulting in significant switching losses. As a follow up, typical soft switching converters operate at very high switching frequencies, resulting reduced dimensions and weights of transformer, filter, and heatsink. For this reason, they are widely diffused in many applications, particularly at low power range (up to few hundred watts) and with fixed load. Numerous integrated circuits embedding power and control circuits in a single chip have been designed for minimizing design efforts and for reducing component count, costs, and dimensions of *LLC* dc/dc converters [2]. High-power applications (kW) require separate power devices and sophisticate control stages implemented in dedicated microprocessors, digital signal processor (DSP) or field programmable gate Arrays [3]. In fact, the occurrence of high amplitude resonant peak voltages and currents and/or the need of large input/output voltage range and load can only be addressed with a sophisticate design. Current literature reports three distinct popular configurations for the resonant dc/dc converters, namely: series resonant converters (SRC), parallel resonant converters (PRC), and series-parallel resonant converters (SPRC) [4].

With reference to SRC topologies, their major problems are the reduced voltage regulation capability at no load condition and their limited short-circuit characteristics. If the input voltage increases, the converter operates away from the

resonant frequency, which leads to more circulating energy in the resonant network instead of being transferred to the load. However, the switching losses decrease when the load decreases [5]. Light load regulation problem does not exist in PRC and because of the resonant circuit inductor, they are short circuit proof. However, the large amount of circulating energy even at light load is a problem for this type of resonant converters [6].

The third category, namely the SPRC resonant converters, combine the advantages of PRC and SRC and eliminate their drawbacks [7], [8]. *LLC* resonant converters, which are the subtype of SPRC, are becoming quite popular in industrial electronics and front-end applications [9]. In comparison with hard switching converters, they have higher efficiency, lower harmonics levels, and produce lower electromagnetic interferences [10]. If properly controlled, they can regulate the output voltage over a large input voltage and load range while maintaining high efficiency [11]. This could be advantageous when dealing with renewable energy sources such as photovoltaic and low-power wind turbine applications or with energy storage systems [12]–[15].

State-space averaging (SSA) and circuit averaging methods are popular approaches in modeling of power electronic converters, but when frequency is much smaller than the switching frequency, they become unreliable [16]. Variations of ac signals should be much smaller than their quiescent operating points, which are not satisfied in resonant converters. Due to nonlinear coupling between ac and dc state variables, series inductor current, magnetizing current, capacitor voltage, and primary transformer voltage of *LLC* resonant converters contain switching frequency harmonics, moreover, the natural frequency of the resonant circuit (also known as "resonant tank") is close to the switching frequency. Hence, SSA and circuit averaging methods cannot be used for modeling this type of converters [17], [18].

Sampled-data modeling is another method in which a steady-state trajectory can be obtained by solving piece-wise linear state equations with respect to the switching boundary conditions [19]. Then, with the same sample interval as the switching period, perturbation and linearization can be performed. The resulting model is accurate, but solution of analytical expressions cannot provide physical insight behavior. Other known methods for modeling and control of resonant converters are: state-plane approach [20], one-cycle control [21], trajectory control [22], [23], and discrete pulse frequency modulation control [24].

In order to derive accurate large signal and small signal models of the *LLC* resonant converter, the Extended Describing Function (EDF) technique [18], [25], [26], based on the first harmonic sinusoidal approximation of the state variables, has been adopted in this study. Modeling and dynamic behavior of the nonlinear system has been obtained replacing each nonlinear element with a describing function whose gain is a function of the input amplitude. Hence, a set of modulating functions relating state variables with control variable and input has been developed [26]. The proposed resonant converter is

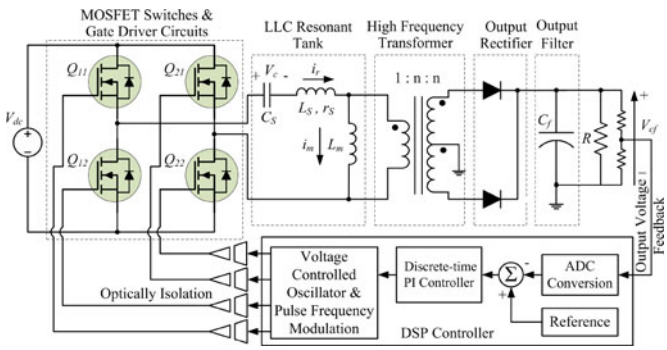

Fig. 1. Configuration of the *LLC* resonant dc/dc converter.

frequency-controlled; however, a model for the duty cycle control or the phase-modulation can also be achieved. A Luenberger-like observer provides to state variables estimation [27]. It has been built up by copying the nonlinear model equations and adding a forcing term, with linear gain, given by the difference between measured output voltage and estimated output voltage. Then, an estimated state feedback controller has been developed. Such state feedback controller involves the current steady-state variables, corresponding to an approximation of current load and input voltage. In particular, a range of input voltage, load, and a quantization step have been considered with the fixed desired output voltage. At each condition, the related steady-state switching frequency and state variables have been computed offline and stored in a lookup table. The observer-based control law is updated at each sampling time, by using the current best approximation of the steady-state switching frequency and state variables, as read from lookup table, selecting a range including the current value of input voltage and load.

In order to validate the concept, a laboratory-scaled prototype of the *LLC* resonant dc/dc converter has been developed. The proposed observer-based controller has been implemented using a DSP microcontroller. The provided method has been compared with a classical Proportional-Integral-Derivative (PID) controller. It has been shown that it outperforms the PID-based counterpart in terms of overshoot and settling time.

The remaining paper is arranged as follows. Section II deals with a description of the approximate nonlinear model of the *LLC* resonant converter. Section III describes in detail the design procedure for obtaining the observer-based controller. Section IV presents and analyze the obtained experimental results. Finally, Section V contains some conclusions.

II. Approximate Nonlinear Model Based on EDF

As shown in Fig. 1, the *LLC* resonant converter consists of four passive components: three in the resonant tank and one in the output filter. To obtain a mathematical model, an approximation technique is needed. Using a sinusoidal approximation, the three ac states in the resonant tank could be decomposed into sine and cosine components. However, this decomposition introduces two states for each ac variable, resulting in a seventh-order dynamic model.

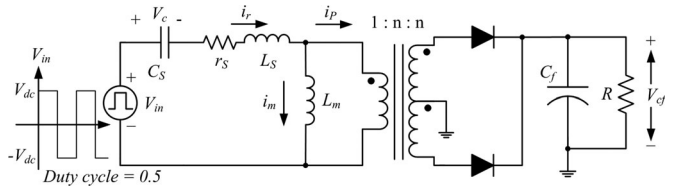

Fig. 2. Equivalent circuit of the *LLC* resonant dc/dc converter.

A. Model Development

Regarding to Fig. 1, a square wave voltage generated from the full-bridge, is applied to the resonant tank of the *LLC* resonant converter. The equivalent circuit is shown in Fig. 2. In this figure, the parasitic resistance of the output capacitor is neglected. The series equivalent resistance of the transformer's primary side is too small (due to design), and the magnetizing current (i_m) is considerably small with respect to the resonant inductor current (i_r). Hence, only series resistance of the resonant inductor is considered for developing the model.

By applying the Kirchhoff's laws to Fig. 2, (1)–(4) could be obtained easily

$$\frac{di_r}{dt} = \frac{1}{L_s}V_{\rm in} - \frac{r_s}{L_s}i_r - \frac{1}{L_s}V_c - \frac{n}{L_s}\text{sign}\left(i_r - i_m\right)V_{cf} \tag{1}$$

$$\frac{dV_c}{dt} = \frac{1}{C_s}i_r \tag{2}$$

$$\frac{di_m}{dt} = \frac{n}{L_m}V_{cf}\text{sign}\left(i_r - i_m\right) \tag{3}$$

$$\frac{dV_{cf}}{dt} = \frac{n}{C_f}\left|i_r - i_m\right| - \frac{1}{R}V_{cf} \tag{4}$$

where $V_{\rm in}$ is a square wave voltage generated from the full-bridge switches to be applied to the resonant tank and i_r, V_c, i_m, and V_{cf} are state variables.

B. Harmonic Approximation

Using the sinusoidal approximation, the three ac state variables i_r, V_c, and i_m in (1)–(4) are decomposed into sine and cosine components, and the derivatives are equated to zero in order to get the steady-state values. However, this decomposition produces two states for each ac variable and leads to a seventh-order dynamic model. Equations (5) and (6) show the approximation for the series resonant current

$$i_r\left(t\right) = i_{rs}\left(t\right)\sin\left(\omega_s t\right) - i_{rc}\left(t\right)\cos\left(\omega_s t\right) \tag{5}$$

$$\frac{di_r}{dt} = \left(\frac{di_{rs}}{dt} + \omega_s i_{rc}\right)\sin\left(\omega_s t\right) - \left(\frac{di_{rc}}{dt} - \omega_s i_{rs}\right)\cos\left(\omega_s t\right). \tag{6}$$

C. Extended Describing Function

The EDF concept is a powerful mathematical method for modeling resonant converters and analyzing their dynamic behavior [26]. This method combines the time domain and frequency domain analysis and extracts the model by dividing modulated waveforms into sine and cosine waveforms. The nonlinear terms, provided in (1)–(4), can be approximated to their fundamental harmonic terms. The EDFs are defined as $F_1\left(d,\, V_{\rm in}\right)$, $F_2(i_s,\, i_p,\, v_{cf})$, $F_3(i_s,\, i_p,\, v_{cf})$, and $F_4(i_s,\, i_c)$

$$F_1\left(d,\, V_{\rm in}\right) = \frac{4V_{\rm dc}}{\pi}\sin\left(\pi d\right) = \frac{4V_{\rm dc}}{\pi} \tag{7}$$

$$F_2\left(i_s,\, i_p,\, v_{cf}\right) = \frac{4}{\pi}\frac{i_s}{i_p}V_{cf} \tag{8}$$

$$F_3\left(i_s,\, i_p,\, v_{cf}\right) = \frac{4}{\pi}\frac{i_c}{i_p}V_{cf} \tag{9}$$

$$F_4\left(i_s,\, i_c\right) = \frac{2}{\pi}i_p \tag{10}$$

where $i_p = \sqrt{\left(i_{rs} - i_{ms}\right)^2 + \left(i_{rc} - i_{mc}\right)^2}$, $i_s = i_{rs} - i_{ms}$, and $i_c = i_{rc} - i_{mc}$ are the sine and cosine components of the transformer secondary current, respectively, and d is the duty cycle which is considered to be 50%. By using (7)–(10), the nonlinear terms of (1)–(4) could be approximated as follows

$$V_{\rm in}\left(t\right) = F_1\left(d,\, V_{\rm in}\right)\sin\left(\omega_s t\right) \tag{11}$$

$$\text{sign(i}_{\rm r} - \text{i}_{\rm m}\text{)V}_{\rm cf} = F_2(i_s, i_p, v_{cf})\sin\left(\omega_s t\right) - F_3\left(i_s,\, i_p,\, v_{cf}\right)\cos\left(\omega_s t\right) \tag{12}$$

$$\left|i_r - i_m\right| = F_4\left(i_s,\, i_c\right). \tag{13}$$

By making use of (7)–(13) from (1)–(4), separating the sine and cosine terms, the following equations are obtained

$$\frac{di_{rs}}{dt} = \frac{4V_{\rm dc}}{\pi L_s} - \omega_s i_{rc} - \frac{r_s}{L_s}i_{rs} - \frac{1}{L_s}v_{cs} - \frac{4n}{\pi L_s}\frac{i_{rs} - i_{ms}}{i_p}V_{cf} \tag{14}$$

$$\frac{di_{rc}}{dt} = \omega_s i_{rs} - \frac{r_s}{L_s}i_{rc} - \frac{1}{L_s}v_{cc} - \frac{4n}{\pi L_s}\frac{i_{rc} - i_{mc}}{i_p}V_{cf} \tag{15}$$

$$\frac{dv_{cs}}{dt} = -\omega_s v_{cc} + \frac{1}{C_s}i_{rs} \tag{16}$$

$$\frac{dv_{cc}}{dt} = \omega_s v_{cs} + \frac{1}{C_s}i_{rc} \tag{17}$$

$$\frac{di_{ms}}{dt} = -\omega_s i_{mc} + \frac{4n}{\pi L_m}\frac{i_{rs} - i_{ms}}{i_p}V_{cf} \tag{18}$$

$$\frac{di_{mc}}{dt} = \omega_s i_{ms} + \frac{4n}{\pi L_m}\frac{i_{rc} - i_{mc}}{i_p}V_{cf} \tag{19}$$

$$\frac{dV_{cf}}{dt} = \frac{2n}{\pi C_f}i_p - \frac{n}{\text{RC}_f}V_{cf}. \tag{20}$$

For obtaining the steady-state operating point, the time derivatives are set to zero, and the output voltage V_{cf} is fixed equal to the desired value. Then, given an input voltage and a load, the corresponding steady-state values of the variables i_{rs}, i_{rc}, v_{cs}, v_{cc}, i_{ms}, i_{mc}, V_{cf} here denoted as $\bar{X} = \left[\bar{I}_{rs}\, \bar{I}_{rc}\, \bar{V}_{cs}\, \bar{V}_{cc}\, \bar{I}_{ms}\, \bar{I}_{mc},\, \bar{V}_{cf}\right]^T$, are obtained, as well as

the steady-state value of the switching frequency ω_s, here denoted as $\bar{\omega}_s$. Though it has not been proved theoretically for any value of the input voltage and the load, the asymptotic stability of $\bar{X}$ has been proved in many cases. Such asymptotic stability has been checked by means of linearization around the equilibrium points $\bar{X}$ [26]. In this regard, input voltage was varied between 65 and 115 V with 5-V steps, and the load was varied between 30 and 130 Ω with 10-Ω steps and output voltage was set to 175 V. For each of these input voltage and load values, the Jacobian matrix, corresponding to the related equilibrium point, always results to have eigenvalues with negative real part.

III. Observer-Based Controller Design and Implementation

A. Proposed Controller

Equations (14)–(20) represent a set of seven nonlinear differential equations in the form

$$\dot{X}(t) = f(X(t), V_{\text{in}}(t), R(t), \omega_s(t)) \tag{21}$$

where $X = [i_{rs}, i_{rc}, V_{cs}, V_{cc}, i_{ms}, i_{mc}, V_{cf}]$ are state variables and ω_s is the control variable. Notice that, the steady state is obtained from the equation in the state-space form (21), by the equation $f(X, V_{\text{in}}, R, \omega_s) = 0$, while V_{in}, R, and seventh component of X are fixed and the first six components of X and ω_s are unknown variables.

In this system, the output voltage V_{cf} is the unique measured state variable, while the other state variables are estimated using the observer described in this section. The observer-based controller utilizes measured values of V_{in} and R which is described in the next section. The state of (21) can be estimated implementing an observer which has been created by making a copy of the original system equations and adding a feedback term from the output error (see [27]). The use of observers for dealing with control of power electronics devices is not new in the literature (see, for instance, [28]–[30]). The observer-based control law is given by

$$\begin{aligned}\dot{\xi}(t) &= f(\xi(t), V_{\text{in}}(t), R(t), \omega_s(t)) + \Gamma(V_{cf}(t) - \xi_7(t)) \\ \omega_s(t) &= \bar{\omega}_s(t) - K\left(\xi(t) - \bar{X}(t)\right)\end{aligned} \tag{22}$$

where $\bar{\omega}_s(t)$ and $\bar{X}(t)$ are the steady-state values at the current input voltage $V_{\text{in}}(t)$ and load $R(t)$, with the fixed desired output voltage V_{cf}. The variables $\xi(t)$ are the estimation of $X(t)$, so that $(\xi(t) - X(t))$ is the estimation error. $\xi_7(t)$ is the estimation of the seventh component of X, that is, the output voltage. The Luenberger-like observer [first row in (22)], has constant gain Γ, as well as the controller (second row) is an estimated state feedback with constant gain K. The block diagram of the system with observer-based controller is shown in Fig. 3.

Since the controller will be implemented using a DSP, equations in (22) should be rewritten in discretized form

$$\begin{aligned}\xi((k+1)\Delta) &= \xi(k\Delta) + \Gamma(V_{cf}(k\Delta) - \xi_7(k\Delta)) \\ &\quad + \Delta f((\xi(k\Delta), V_{\text{in}}(k\Delta), R(k\Delta), \omega_s(k\Delta)) \\ \omega_s(k\Delta) &= \bar{\omega}_s(k\Delta) - K\left(\xi(k\Delta) - \bar{X}(k\Delta)\right)\end{aligned} \tag{23}$$

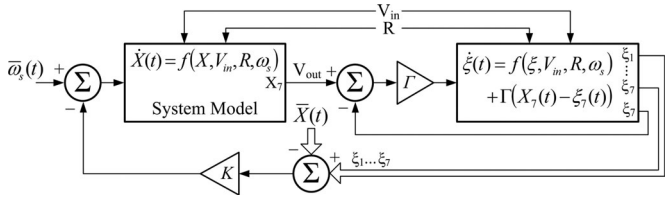

Fig. 3. System function block diagram with observer-based control.

where $\bar{\omega}_s(k\Delta)$ and $\bar{X}(k\Delta)$ are the best approximations for steady-state values of ω_s and X at kth sample, taken from the lookup table containing values corresponding to the current input voltage and load.

B. Implementation

The closed-loop system has been realized by initializing the observer at the steady-state value $\bar{X}$, which is available at the current input voltage and load, by means of the model previously described in (21).

For computation of (22), the Euler approximation method is used [see (23)]. Alternatively, better methods, like Runge–Kutta [31], could be adopted but at the cost of higher computational time. Nevertheless, it can be noticed that the proposed observer-based controller of (22) can be very easily implemented in a DSP by means of (23), and even by using the lookup table it yields very good results.

The constant gains of the observer and of the estimated state feedback control law are mostly found by means of experimental trials, starting from values provided by MATLAB ACKER command for the linearized (system and observer) models. The values of Γ and K, found experimentally, are such that the dynamic matrix describing the linearized closed-loop system is Hurwitz. A table of input voltages and load values are built, and for each of the points, the corresponding steady state is computed. This is the lookup table which is used when implementing (23), in order not to lose time for computing the steady state. The best approximation of the steady state corresponding to current input voltage and load are taken from the lookup table.

It should be emphasized that the lookup table for the steady-state values of state variables and switching frequency are done only using (21) and without performing any experiment. As well, the gains of the observer and of the estimated state feedback are tuned once and are not changed for the different load and input voltage situations.

At each sampling time, the controller has to perform the following steps: 1) read the current input voltage, output voltage, and load; 2) by using lookup table: read the steady-state switching frequency and state variables corresponding to the range including the current input voltage and load; 3) compute the control law [i.e., $\omega_s(k\Delta)$ in (23)], to be applied in the sampling interval by zero-order hold; 4) compute the estimated state variable by Euler approximation, for next sampling time [i.e., $\xi((k+1)\Delta)$ in (23)].

In this study, input voltage range has been chosen between 65 and 115 V with 5-V steps, and the load range has been

TABLE I
PARAMETERS OF THE *LLC* DC/DC RESONANT CONVERTER

Parameter	Description	Value
$V_{\rm dc}$	Nominal input dc voltage [V]	90
$V_{\rm out}$	Nominal output dc voltage [V]	200
$I_{\rm out}(\max)$	Maximum output current [A]	7.5
L_s	Resonant tank conductance [μH]	13.1
C_s	Resonant tank capacitor [nF]	170
L_m	Magnetizing conductance [μH]	47
n	Transformer ratio	1.875
C_f	Output capacitor [μF]	2 * 33
f_r	Resonant frequency [kHz]	106.7

chosen between 30 and 130 Ω with 10-Ω steps. The observer-based controller in (23) is implemented by using the steady-state values of $\bar{\omega_s}$ and $\bar{X}$ at different values of the input voltage $V_{\rm in}$ and load R as best approximated in the lookup table. Gain vector Γ and control gain K have been adjusted by means of experiments and the following well working gains are found

$$\Gamma = [0.2 \quad 0.2 \quad 0.3 \quad -0.1 \quad -0.25 \quad 0.6 \quad 0.8]^T \quad (24)$$

$$K = [2 \quad 25 \quad 4 \quad -0.25 \quad -30 \quad 6 \quad 2]. \quad (25)$$

IV. EXPERIMENTAL RESULTS AND ANALYSIS

Specifications of the parameters used for the model, shown in Fig. 1, are given in Table I.

For the experiments, a 1.5-kW laboratory prototype of a full-bridge *LLC* resonant dc/dc converter has been built. Another auxiliary test board has been designed and created to apply load and input voltage changes as step function at the precise times. Texas Instruments Piccolo TMS320F28069 control card [32] which contains a 32-bit floating point DSP microcontroller, has been used to implement control algorithms, produce pulse frequency modulation for power MOSFET switches, and command the auxiliary board. For implementing both the PID and the proposed observer-based controllers in DSP, these control algorithms have been written on high level language C by using TI's Code Composer Studio (CCS) with or without activated Floating Point Unit (FPU) configuration for F28069 device. Then, the generated machine code was programmed into on-chip RAM memory by CCS to execute the instruction code from it. Fig. 4 shows the experimental setup indicating each unit mentioned above.

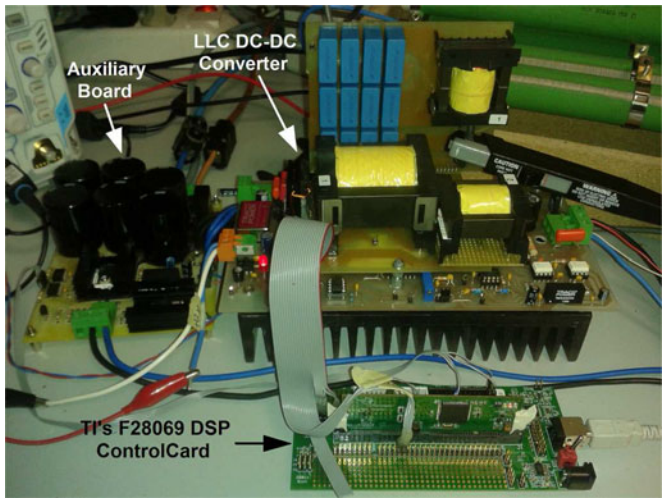

Fig. 4. Experimental setup of 1.5-kW *LLC* resonant dc/dc converter.

A. Operation and Open-Loop Transient and Frequency Responses of the LLC Resonant DC/DC Converter

In this section, a brief study of general operation, open-loop transient and frequency responses of the *LLC* resonant converter is presented. At first, to show ZVS operation of MOSFET switches, switching waveforms of *LLC* resonant tank are shown in Fig. 5. All of these experiments were performed without controller, and the output power is set to 700 W with 180-V output voltage.

Fig. 5(a) presents Q_{11} MOSFET's voltage and current waveforms at frequency above resonant frequency (f_r). As shown in this figure at the switch-on time, its current is negative, which is flowing through the reverse body diode of MOSFET and maintains its drain-source voltage about 0 V at this moment. This behavior ensures the ZVS turn-on in all power MOSFET switches. Resonant *LLC* tank voltage and current switching waveforms at frequencies lower and higher than f_r are also shown in Fig. 5(b) and (c), respectively. ZVS operation of the switches is obvious in these figures, as well. It should be noted that, in Fig. 5(c), ZVS is achieved by flowing the magnetizing current of L_m through reverse body diode and should be large enough to ensure ZVS in all operation range of converter by taking into account the dead-band time.

The control frequency-to-output voltage transient response of the resonant dc/dc converter prototype without controller is shown in Fig. 6. In this test, large step changes were applied to control signal (switching frequency) by DSP at the specified times. The test condition were as follows: input voltage $V_{\rm dc} = 90\,{\rm V}$, output voltage at resonant frequency $V_{\rm out} = 171\,{\rm V}$, and output resistance $R_{\rm out} = 77\,\Omega$. In this figure, upper graph shows the converter output voltage, and lower graph indicates the *LLC* tank resonant current. At first, switching frequency was set to resonant frequency ($f_r = 106.67\,{\rm kHz}$), then suddenly increased to $1.25\ f_r$ (133.33 kHz) at $t = 2\,{\rm ms}$. Then, at $t = 5\,{\rm ms}$ and $t = 8\,{\rm ms}$, it decreased to $0.83\ f_r$ (88.89 kHz) and increased again to $1.25\ f_r$ as a step, respectively. It can be seen from this figure, transient responses to step function have different settling time without any overshoot. Furthermore, for 25% increase of switching frequency there is about 15 V drop, and for 17% decrease in switching frequency there is about 26 V rise in output voltage. These results demonstrate the nonlinearity of the *LLC* resonant dc/dc converter.

Knowing the open-loop frequency response of the actual system is one of the key benefits to understand the system dynamics. To achieve frequency response of the *LLC* resonant converter, a pure sinusoidal signal with different frequencies should be injected to control signal (switching frequency) with proper dc offset equal to resonant frequency to maintain switching

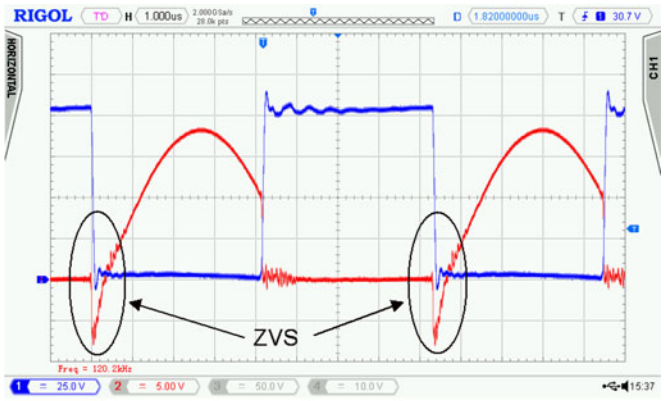

(a)

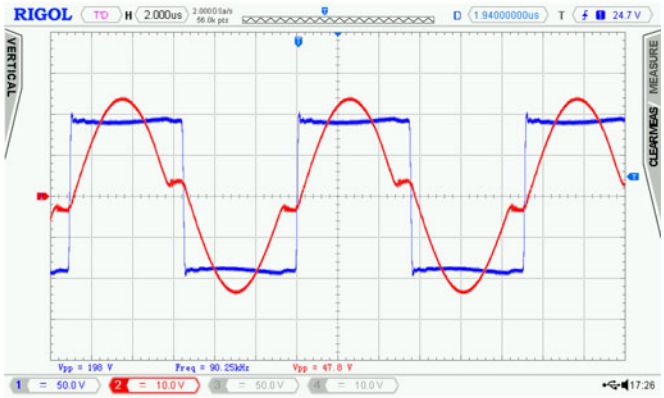

(b)

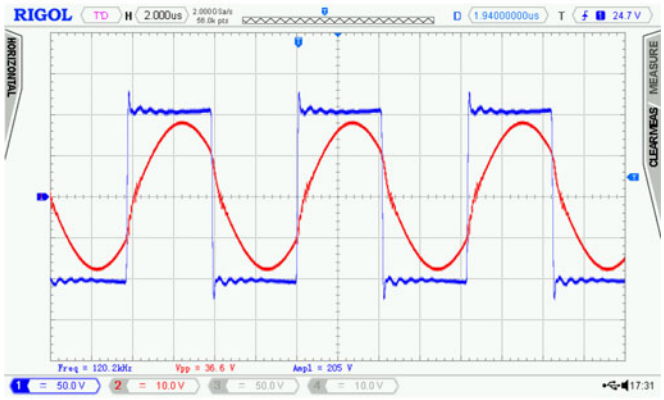

(c)

Fig. 5. *LLC* resonant dc/dc converter operation waveforms. (a) Voltage and current waveforms of MOSFET Q_{11} at frequency above f_r (CH1 (square waveform): 25 V/div, CH2: 5 A/div, Time: 1 μs/div). (b) Resonant *LLC* tank voltage and resonant inductor current at frequency below f_r (CH1 (square waveform): 50 V/div, CH2: 10 A/div, Time: 2 μs/div). (c) Resonant *LLC* tank voltage and resonant inductor current at frequency above f_r (CH1 (square waveform): 50 V/div, CH2: 10 A/div, Time: 2 μs/div).

frequency variation just around the resonant frequency. Then, at each injected signal, with certain amplitude and frequency, the output amplitude and phase difference are measured for the specific frequency. To extract frequency response (Bode diagram) of created resonant dc/dc converter, Stanford Research Systems network signal analyzer (Model SR780) has been used. A program has been developed by TI's Code Composer on Piccolo F28069 DSP controller to manage source signal produced by network analyzer and DC offset. Final applied signal to Voltage-Controlled Oscillator (VCO), which has been implemented inside the DSP is as follows:

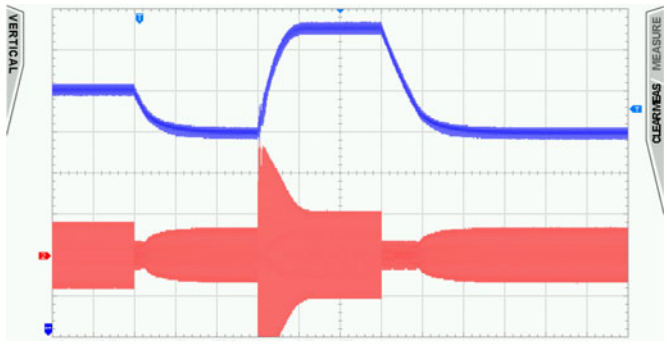

Fig. 6. Control to output transient of the converter, Top: output voltage (15V/div), Bottom: LLC tank resonant current (10A/div), Time: 1*ms*/div.

$$f_{\mathrm{VCO}} = f_r + A_s \sin\left(2\pi f_s t\right) \cdot 25000 \tag{26}$$

where f_{VCO} and f_r are VCO and resonant frequencies, A_s and f_s are network analyzer source signal amplitude and frequency, respectively. To measure transfer function or frequency response, A_s was set to 200 mV and f_s was varied between 40 Hz and 100 kHz. Fig. 7 shows the control to output frequency response of the open-loop system (without controller) for *LLC* resonant converter laboratory prototype. In Fig. 7(a), the marked point indicates -3 dB cutoff frequency which is about 1400 Hz. In Fig. 7(b), the phase starts from 180° which represents inverse operation of system (the output voltage decreases by increasing the control switching frequency). As seen from this figure, the phase is decreased significantly at higher frequencies because the conversion delay time of ADC by DSP becomes sensible in these frequencies. The same frequency response extraction test has been performed by MATLAB/Simulink to verify the experimental test, which is shown in Fig. 8.

B. Results

For the comparison purpose, a PID controller has also been implemented. Proportional, integral, and derivative gain parameters of the PID controller are summarized in Table II and were calculated according to Ziegler–Nichols tuning method [33]. To calculate these parameters, at first, K_I and K_D were set to zero, and K_P was increased until the output voltage starts to oscillate without damping. This procedure has been performed by using MATLAB/Simulink and considering actual parameters of the system converter power MOSFET switches and inductors in the simulation. This simulation result is shown in Fig. 9 and the parameters K_u (the value of K_P when output starts to oscillate) and T_u (the period of oscillation) were obtained as $K_u = 0.15$ and $T_u = 257\,\mu$s, respectively. Afterward, a fine adjustment on gain parameters were done by trial-and-error method, experimentally, to modify controller parameters to achieve better transient responses. These parameters were set to $K_P = 0.082$, $K_I = 575$, and $K_D = 5.5e-6$. The discrete

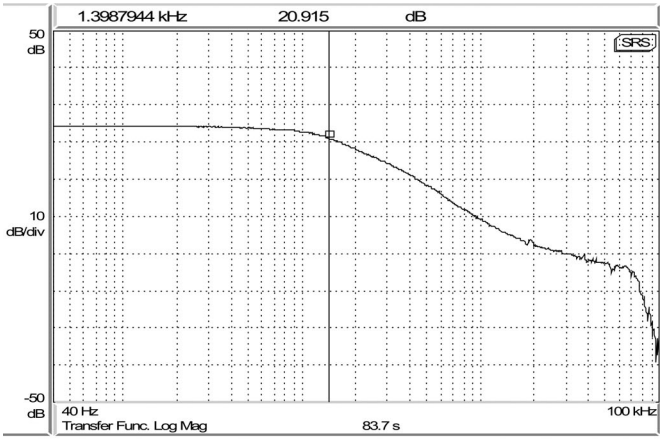

(a)

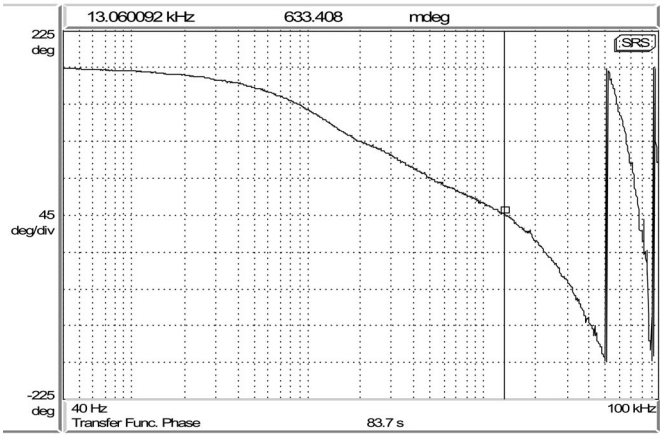

(b)

Fig. 7. Experimental open-loop control to output frequency response (Bode diagram) of the resonant dc/dc converter. (a) Gain (db) vs. frequency and (b) Phase (degree) vs. frequency.

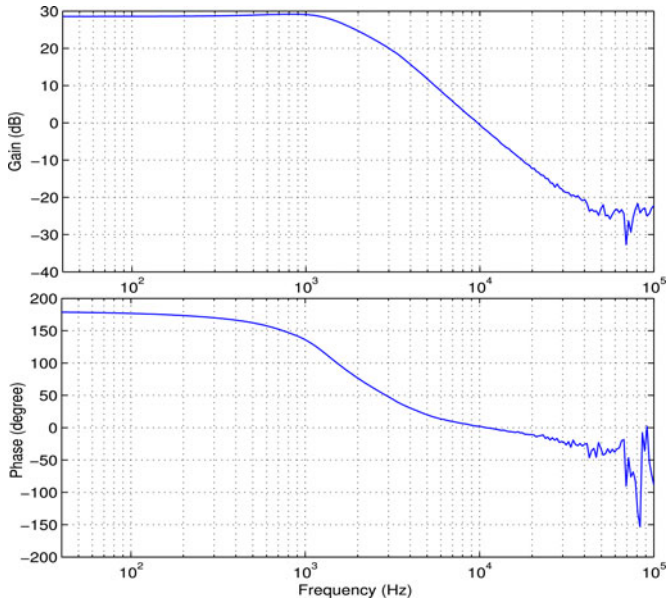

Fig. 8. Simulated open loop control to output frequency response (Bode diagram) of the resonant dc/dc converter.

TABLE II
ZIEGLER–NICHOLS PARAMETERS FOR PID CONTROLLER

Control Type	K_P	K_I	K_D
PID	$0.6K_u$	$2\frac{K_P}{T_u}$	$K_P\frac{T_u}{8}$
	0.09	700	$2.9e-6$

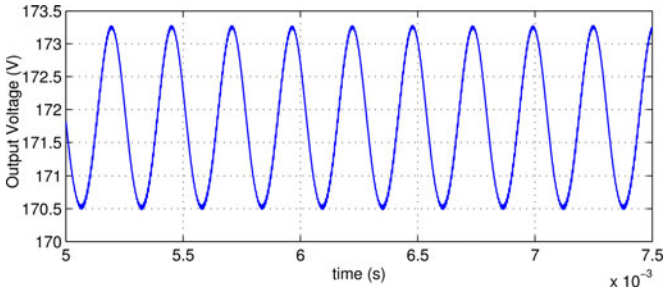

Fig. 9. Simulation results for Ziegler–Nichols method.

TABLE III
EXECUTION TIME OF CONTROL ALGORITHMS BY USING PICCOLO F28069 AT 80-MHZ CLOCK SPEED

Controller	**Execution Time** $[\mu s]$	
	without FPU	with FPU
PID	39.8	4.32
Observer-based	148	19.2

PID (see Appendix) and the observer-based controller operate with a sampling time of $20\,\mu$s. Regarding the converter open-loop transient and frequency responses, illustrated in Figs. 6 and 7, this control sampling time is enough for controller response to any disturbances such as input voltage and/or output load changes.

The execution times, operating at 80-MHz clock speed, are given in Table III. As seen from these results, the execution time of both PID and the proposed control algorithms are small enough by using FPU calculations. On the other hand, the cost of the adopted DSP (less than USD 5) is more than reasonable taking into account achievable results.

Fig. 10(a) and (b) shows the transient responses of the *LLC* resonant dc/dc converter prototype versus output load (current) change for PID and observer-based controllers, respectively. In these tests, the desired output voltage was set to 175 V, and output current was suddenly changed as a step change from 2.28(about 400 -W output power) to 5.57 A (about 975-W output power), and vice versa. As seen in these figures, output voltage drops are about 15 V and 8 V at the rising edge of current, and output voltage rises at falling edge of current are 8 and 6 V for PID and observer-based controllers, respectively. Furthermore, the PID controller responds to output current disturbances with a settling time of 1.2 and 1.5 ms for rising and falling edges, and the observer-based controller responds with a settling time of

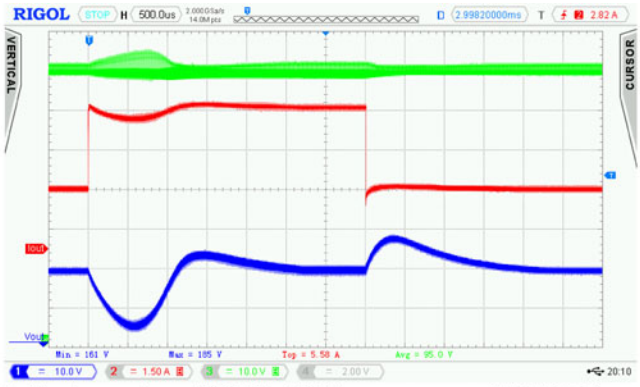

(a) Top: input voltage (10V/div), Middle: output current (1.5A/div), Bottom: output voltage (10V/div), Time: 500μs/div.

(b) Top: input voltage (10V/div), Middle: output current (1.5A/div), Bottom: output voltage (10V/div), Time: 500μs/div.

Fig. 10. Transient response of the converter against step changes in output load with: (a) PID controller, (b) proposed controller.

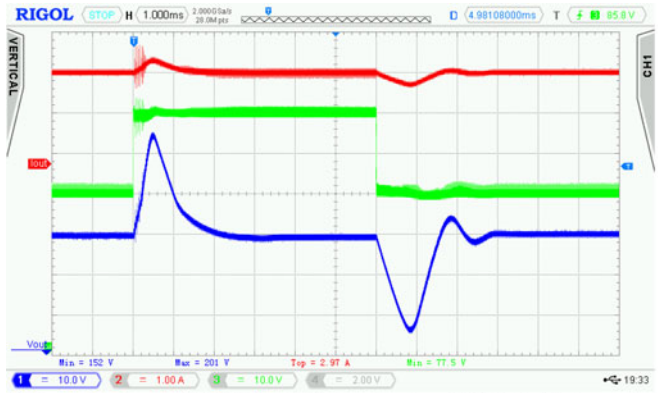

(a) Top: output current (1A/div), middle: input voltage (10V/div), Bottom: output voltage (10V/div), Time: 1ms/div.

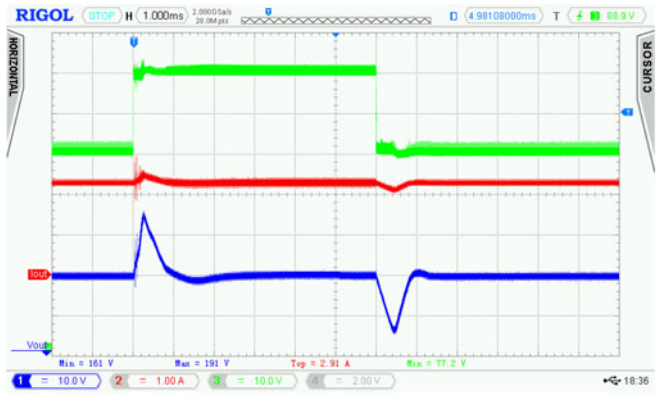

(b) Top: input voltage (10V/div), middle: output current (1A/div), Bottom: output voltage (10V/div), Time: 1ms/div.

Fig. 11. Transient response of the converter against step changes in input voltage with: (a) PID controller, (b) proposed controller.

0.4 ms in both cases. These experiments demonstrate the better performance of the proposed observer-based controller over PID controller.

In order to evaluate each controller performance, another transient response test has been done according to input voltage variations. In this test, the desired output voltage has been also set to 175 V and 20 V step-up and step-down changes have been applied to input voltage of the *LLC* resonant dc/dc converter. The obtained experimental results against these variations are shown in Fig. 11(a) and (b) for PID and observer-based controllers. As shown in these figures, output voltage variations with respect to input voltage disturbances are about 25 and 14 V for PID and proposed controller, respectively. Moreover, the output voltage reaches its steady-state stable value in 2 and 3 ms for rising and falling edges, respectively with PID controller, and this time is just 0.9 ms for the observer-based controller in both cases. It is evident from experimental results that the proposed observer-based controller has better transient response than the tuned PID controller. To see how much bandwidth or stability is gained by the proposed method, the bode diagram of closed-loop system for observer-based and PID controllers is extracted by simulation which is shown in Fig. 12. Notice that with the proposed observer-based controller, the bandwidth is significantly increased with respect to the PID case. In general, larger bandwidth corresponds to shorter rise time. Indeed, shorter transient is shown clearly by experiments for the method presented here, with respect to the PID methodology.

Finally, Fig. 13 shows the efficiency of the converter prototype versus output power. The proposed *LLC* converter has quite good efficiency in wide range of output power especially at lower output power levels. Regarding the figure, the output power is changed from 200 to 1000 W with output voltage fixed at 175 V. The switching frequency varies from about 124 kHz to 105 kHz with respect to this change. For the powers beyond this criteria, the switching frequency of the converter is bounded within 95–175 kHz interval. The low boundary is set to ensure ZVS operation, and the high boundary is set to protect gate drivers and MOSFETs from failure.

As illustrated in Figs. 10 and 11, the transient responses of the observer-based controller are better in comparison with PID controller. So, during transients the energy absorbed by the converter is smaller with the proposed controller which results in better efficiency. In this study, our major concern was design of a proper controller rather than efficiency optimization. However the obtained values can be improved with a more accurate realization (i.e., designing the optimized high frequency inductor and transformer) to reach higher efficiency. Moreover, by paralleling the power switches and/or using faster and lower

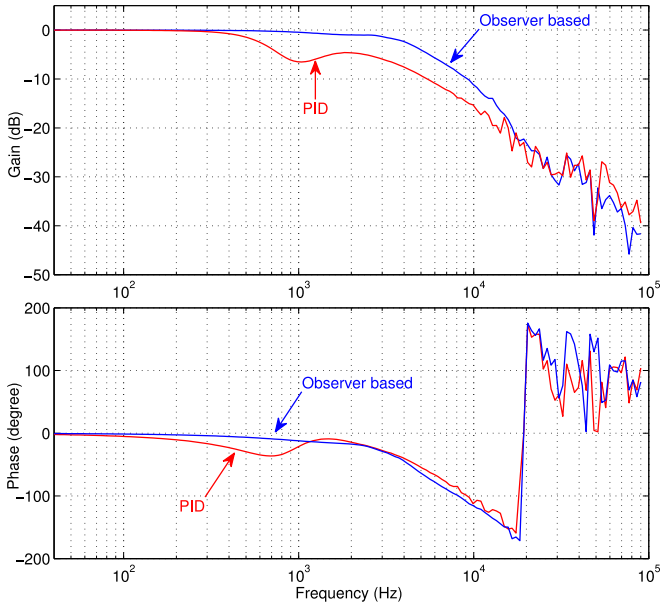

Fig. 12. The bode diagram of the closed loop system for observer-based and PID controllers.

drain-source on-resistance MOSFETs, the switching and conduction losses can be greatly decreased.

V. Conclusion

This paper addressed theoretical and practical issues regarding the dynamic analysis and control design of the *LLC* resonant dc/dc converter operating under large input voltage and load variations. Since the switching frequency of the *LLC* resonant converter is in the vicinity of the resonant frequency, typical approaches such as the SSA method cannot be used. In this paper, an accurate model has been developed using the EDF method, which combines time domain and frequency domain analysis and extracts the model by dividing modulated waveforms into sine and cosine waveforms. Detailed procedures to obtain such an approximate model have been presented and discussed.

The derived model is then used to design an observer-based controller. The experimental results showed that the proposed controller is effective in stabilizing the output voltage under various situations of input voltage as well as load. The dynamic responses under sudden changes of input and output are compared with the classic PID controller. Experimental studies proved the superiority of the proposed observer-based controller over PID controller.

Appendix

The converter block diagram controlled by a discrete-time PID controller is shown in Fig. 14.

Backward Euler method, also known as Backward Rectangular or right-hand approximation was used to realize the integrator term [33]. With this method, the integrator is approximated by $T_s Z/(Z-1)$. The discrete-time output of the integrator at step n is $u_I(n) = u(n-1) + K_I T_s e(n)$.

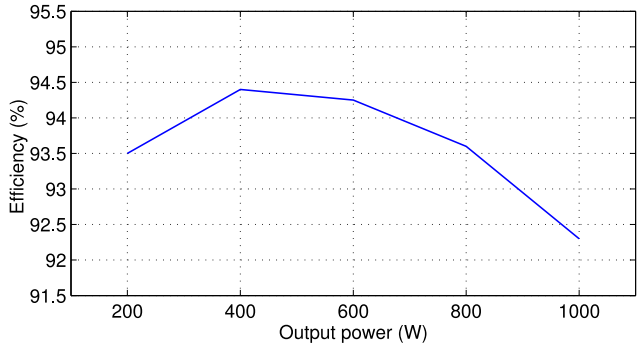

Fig. 13. Efficiency of the prototype versus output power.

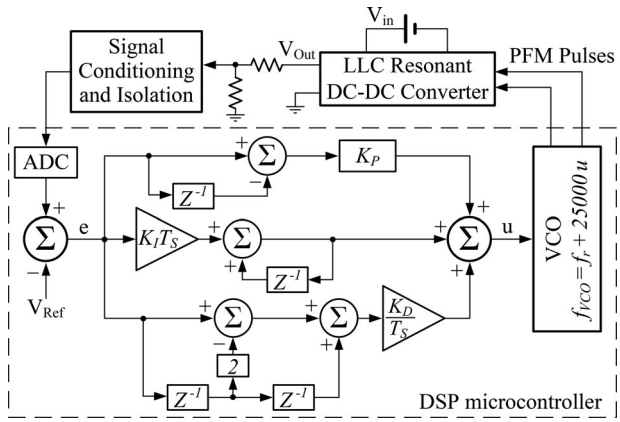

Fig. 14. Block diagram of the converter with discrete time PID controller.

Consequently, the expression of the output of the discrete-time PID controller at step n is as follows:

$$\begin{aligned} u(n) &= u(n-1) + (K_P + K_I T_s + K_D/T_s)\, e(n) \\ &\quad + (-K_P - 2K_D/T_s)\, e(n-1) \\ &\quad + K_D/T_s\, e(n-2) \end{aligned} \tag{27}$$

where $e(n)$ and $u(n)$ represent the error signal and output of the controller at step n, respectively.

Sampling time was set to $20\,\mu$s and a 5-kHz fourth-order Butterworth low-pass filter was included in order to reduce input signal bandwidth.

Acknowlegement

The authors would like to thank F. Mancini for his supports and helps in workshop especially in preparing printed circuit boards for prototype implementations.

References

[1] Y. Gu, Z. Lu, L. Hang, Z. Qian, and G. Huang, "Three-level LLC series resonant DC/DC converter," *IEEE Trans. Power Electron.*, vol. 20, no. 4, pp. 781–789, Jul. 2005.

[2] http://www.irf.com/product/DC-DC-Converters-Integrated-POL-Converters/_/N~1nje1i#tab-tab1

[3] C. Buccella, C. Cecati, and H. Latafat, "Digital control of power converters—A survey," *IEEE Trans. Ind. Inform.*, vol. 8, no. 3, pp. 437–447, Aug. 2012.

[4] M. K. Kazimierczuk and D. Czarkowski, *Resonant Power Converters*, 2nd ed. Hoboken, NJ, USA: Wiley-Interscience, 2011.

[5] M. K. Kazimierczuk and S. Wang, "Frequency-domain analysis of series resonant converter for continuous conduction mode," *IEEE Trans. Power Electron.*, vol. 7, no. 2, pp. 270–279, Apr. 1992.
[6] Y. G. Kang, A. K. Upadhyay, and D. L. Stephens, "Analysis and design of a half-bridge parallel resonant converter operating above resonance," *IEEE Trans. Ind. Appl.*, vol. 27, no. 2, pp. 386–395, Mar./Apr. 1991.
[7] J. L. Sosa, M. Castilla, J. Miret, L. G. de Vicuna, and J. Matas, "Modeling and performance analysis of the DC/DC series-parallel resonant converter operating with discrete self-sustained phase-shift modulation technique," *IEEE Trans. Ind. Electron.*, vol. 56, no. 3, pp. 697–705, Mar. 2009.
[8] A. Aboushady, K. H. Ahmed, S. J. Finney, and B. W. Williams, "Linearized large signal modeling, analysis, and control design of phase-controlled series-parallel resonant converters using state feedback," *IEEE Trans. Power Electron.*, vol. 28, no. 8, pp. 3896–3911, Aug. 2013.
[9] X. Li, "A LLC-Type dual-bridge resonant converter: Analysis, design, simulation, and experimental results," *IEEE Trans. Power Electron.*, vol. 29, no. 8, pp. 4313–4321, Aug. 2014.
[10] C. Buccella, C. Cecati, H. Latafat, and K. Razi, "Comparative transient response analysis of LLC resonant converter controlled by adaptive PID and fuzzy logic controllers," in *Proc. IEEE Int. Conf. Ind. Electron. Soc.*, 2012, pp. 4729–4734.
[11] H. Hu, X. Fang, F. Chen, Z. J. Shen, and I. Batarseh, "A modified high-efficiency LLC converter with two transformers for wide input-voltage range applications," *IEEE Trans. Power Electron.*, vol. 28, no. 4, pp. 1946–1960, Apr. 2013.
[12] C. H. Chang, E. C. Chang, and H. L. Cheng, "A high-efficiency solar array simulator implemented by an LLC resonant DC/DC converter," *IEEE Trans. Power Electron.*, vol. 28, no. 6, pp. 3039–3046, Jun. 2013.
[13] F. Musavi, M. Craciun, D. S. Gautam, W. Eberle, and W. G. Dunford, "An LLC resonant DC–DC converter for wide output voltage range battery charging applications," *IEEE Trans. Power Electron.*, vol. 28, no. 12, pp. 5437–5445, Dec. 2013.
[14] T. LaBella, Y. Wensong, L. Jih-Sheng, M. Senesky, and D. Anderson, "A bidirectional-switch-based wide-input range high-efficiency isolated resonant converter for photovoltaic applications," *IEEE Trans. Power Electron.*, vol. 29, no. 7, pp. 3473–3484, Jul. 2014.
[15] C. Buccella, C. Cecati, H. Latafat, and K. Razi, "A grid-connected PV system with LLC resonant DC-DC converter," in *Proc. Int. Conf. Clean Electr. Power*, Jun. 2013, pp. 777–782.
[16] J. Sun, D. M. Mitchell, M. F. Greuel, P. T. Krein, and R. M. Bass, "Averaged modeling of PWM converters operating in DCM," *IEEE Trans. Power Electron.*, vol. 16, no. 4, pp. 482–492, Jul. 2001.
[17] M. K. Kazimierczuk, *Pulse-Width Modulated DC-DC Power Converters*. Oxford, U.K., Wiley, 2008.
[18] E. C. Chang, C. A. Cheng, H. L. Cheng, and S. C. Lin, "Small signal modeling of LLC resonant converters based on extended describing function," in *Proc. Int. Symp. Comput., Consumer Control*, Jun. 2012, pp. 365–368.
[19] G. C. Verghese, M. E. Elbuluk, and J. G. Kassakian, "A general approach to sampled-data modeling of power electronic circuits," *IEEE Trans. Power Electron.*, vol. 1, no. 2, pp. 76–89, Apr. 1986.
[20] R. Oruganti and F. C. Lee, Resonant power processors, Part I–State-Plane analysis, " *IEEE Trans. Ind. Appl.*, vol. IA-21, no. 6, pp. 1453–1460, Nov. 1985.
[21] K. M. Smedley and S. Cuk, "One cycle control of switching converters," *IEEE Trans. Power Electron.*, vol. 10, no. 6, pp. 625–633, Nov. 1995.
[22] W. Feng, F. C. Lee, and P. Mattavelli, "Optimal trajectory control of burst mode for LLC resonant converter," *IEEE Trans. Power Electron.*, vol. 28, no. 1, pp. 457–466, Jan. 2013.
[23] W. Feng and F. C. Lee, "Optimal trajectory control of LLC resonant converters for soft start-up," *IEEE Trans. Power Electron.*, vol. 29, no. 3, pp. 1461–1468, Mar. 2014.
[24] H. Ma, Q. Liu, and Y. Wang, "Discrete pulse frequency modulation control with sliding-mode implementation on LLC resonant DC/DC converter via input-output linearization," *IET. Power Electron.*, vol. 7, no. 5, pp. 1033–1043, May 2014.
[25] A. Ayachit, D. Murthy-Bellur, and M. K. Kazimierczuk, "Steady-state analysis of series resonant converter using extended describing function method," in *Proc. Int. Midwest Symp. Circuits Syst.*, Aug. 2012, pp. 1160–1163.
[26] C. Buccella, C. Cecati, H. Latafat, P. Pepe, and K. Razi, "Linearization of LLC resonant converter model based on extended describing function concept," in *Proc. IEEE Int. Workshop Intell. Energy Syst.*, Nov. 2013, pp. 131–136.
[27] E. D. Sontag, *Mathematical Control Theory: Deterministic Finite Dimensional Systems*, 2nd ed. New York, NY, USA: Springer, 1998.
[28] C. Wang, X. Li, L. Guo, and Y. W. Li, "A nonlinear-disturbance-observer-based DC-Bus voltage control for a hybrid AC/DC microgrid," *IEEE Trans. Power Electron.*, vol. 29, no. 11, pp. 6162–6177, Nov. 2014.
[29] A. B. Youssef, S. K. El Khil, and I. Slama-Belkhodja, "State observerbased sensor fault detection and isolation, and fault tolerant control of a single-phase PWM rectifier for electric railway traction," *IEEE Trans. Power Electron.*, vol. 28, no. 12, pp. 5842–5853, Dec. 2013.
[30] P. Peltoniemi, P. Nuutinen, and J. Pyrhonen, "Observer-based output voltage control for DC power distribution purposes," *IEEE Trans. Power Electron.*, vol. 28, no. 4, pp. 1914–1926, Apr. 2013.
[31] X. Y. Li and C. M. Chen, "Solving nonlinear equations by Runge-Kutta method," *Math. Theory Appl.*, vol. 28, no. 2, pp. 62–65, 2008.
[32] [Online]. Available: http://www.ti.com/tool/tmdscncd28069iso
[33] V. Bobal, J. Böhm, J. Fessl, and J. Machacek, *Digital Self Tuning Controllers Algorithms Implementation and Applications.* London U.K.: Springer-Verlag, 2005.

Concettina Buccella (M'92–SM'03) received the Dr.Eng. degree from the University of L'Aquila, L'Aquila, Italy, and the Ph.D. degree from the University of Rome "La Sapienza", Rome, Italy, both in electrical engineering.

From 1988 to 1989, she was with Italtel S.p.A., then, she joined the University of L'Aquila, where since 2001 she is an Associate Professor. Her research interests include power electronics and their applications to power systems, smart grids, electromagnetic compatibility, electrostatic processes and ultrawide-band signal interferences. She is the C.E.O. of DigiPower Ltd., an university spin-off dealing with industrial electronics and renewable energies.

Dr. Buccella was a corecipient of the 2012 and 2013 IEEE TRANSACTIONS ON INDUSTRIAL INFORMATICS Best Paper Award.

Carlo Cecati (M'92–SM'03–F'06) received the Dr.Ing. degree in electrotechnical engineering from the University of L'Aquila, L'Aquila, Italy, in 1983.

Since then, he has been with the University of L'Aquila, where since 2006 he has been a Full Professor. Since 2014, he has been also the Chief International Academic Adviser at Harbin Institute of Technology, Harbin, China. In 2007, he was a cofounder of DigiPower Ltd. and he is currently the Technical Director. His research and technical interests include several aspects of power electronics, electrical drives, digital control, distributed generation, and smart grids. Since 2013

Prof. Cecati is the Editor-in-Chief of the IEEE TRANSACTIONS ON INDUSTRIAL ELECTRONICS.

Hamed Latafat (S'11) was born in Tabriz, Iran. He received the B.Sc. and M.Sc. degrees in electrical engineering from the University of Tabriz, Tabriz, in 2005 and 2008, respectively, and the Ph.D. degree in energy optimization and sustainable building from University of L'Aquila, L'Aquila, Italy, in 2014.

During the Ph.D. studies, he was also a Visiting Scholar at the University of Texas at Dallas, Richardson, TX, USA. His main research interests include development of power electronic converters, application of power electronics to renewable energy systems and smart grids, implementation of control techniques using microcontrollers, digital signal processor, and field programmable gate array.

Pierdomenico Pepe (M'03–SM'06) received the Laurea degree in electronic engineering (summa cum laude) from the University of Ancona, Ancona, Italy, in 1990, and the Ph.D. degree in electronic engineering from the University of L'Aquila, L'Aquila, Italy, in 1996.

He is currently an Associate Professor at the University of L'Aquila. His main research interests include stability theory, nonlinear control, observers, optimal control, with special emphasis to systems with time-delays, and to applications in biomedical, chemical, electrical and mechanical engineering.

Dr. Pepe has served as IPC Member in several (IFAC, IEEE, SIAM) international conferences. He is currently serving as an Associate Editor of the IEEE TRANSACTIONS ON AUTOMATIC CONTROL, the IEEE SYSTEMS AND CONTROL LETTERS, and the IEEE JOURNAL ON CONTROL AND DECISION.

Kaveh Razi (S'12) was born in Tabriz, Iran. He received the B.Sc. degree from Islamic Azad University, Tabriz Branch, Tabriz, Iran, in electronic engineering and the M.Sc. degree from the University of Tabriz, Tabriz, in power electronics in 2005 and 2008, respectively. He is currently working toward the Ph.D. degree at the University of L'Aquila, L'Aquila, Italy.

His research interests include the development of power electronics converters, renewable photovoltaic systems, artificial intelligence applications, and digital control using microcontrollers, digital signal processors, and field programmable gate arrays.